

247 nm solar-blind ultraviolet *p-i-n* photodetectorV. V. Kuryatkov, B. A. Borisov, and S. A. Nikishin^{a)}*Department of Electrical and Computer Engineering, Texas Tech University, Lubbock, Texas 79409*

Yu. Kudryavtsev and R. Asomoza

SIMS Laboratory of SEES, Department of Electrical Engineering, CINVESTAV, Mexico Distrito Federal 07300, Mexico

V. I. Kuchinskii and G. S. Sokolovskii

Ioffe Physico-Technical Institute, 26 Polytechnicheskaya, St. Petersburg 194021, Russian Federation

D. Y. Song and M. Holtz

Department of Physics, Texas Tech University, Lubbock, Texas 79409

(Received 8 May 2006; accepted 24 August 2006; published online 6 November 2006)

We describe solar-blind *p-i-n* photodetectors based on short period superlattices of AlN/Al_{0.08}Ga_{0.92}N. The devices are grown using gas source molecular beam epitaxy with ammonia on transparent sapphire substrates. The cutoff wavelength for the device is 247 nm. For diodes with 150 μm diameter mesas and sidewall surfaces passivated in oxygen plasma, we obtain extremely low dark leakage current of ~3 pA/cm² and high zero-bias resistance of ~6 × 10¹⁴ Ω. At 10 V reverse bias the observed responsivity is 62 mA/W. © 2006 American Institute of Physics. [DOI: 10.1063/1.2364049]

AlGaN-based solar-blind photodetectors (PDs) have been demonstrated recently.^{1–3} Device designs with response in the 240–290 nm (5.17–4.28 eV) range require *n*-type, intrinsic, and *p*-type AlGaN with AlN mole fractions of 0.5 and higher. High performance *p-i-n* PD structures designed for back illumination must be grown on UV transparent substrates. The *i* region must absorb light in the desired wavelength range and be sandwiched by wider band gap (transparent) *n*- and *p*-type cladding regions.

PDs based on AlGaInN alloys have been grown primarily by metal organic chemical vapor deposition (MOCVD).^{4,5} However, forming high quality AlGaN *p-i-n* structures which exhibit low leakage current and desirable *p*-type doping level is difficult at high AlN mole fraction. One major problem is the high defect density due to substrate-lattice mismatch. The second problem is the large acceptor activation energy of *p*-type dopant Mg in high Al content alloys. We have shown that short period superlattices (SPSLs) of AlN/Al_{0.08}Ga_{0.92}N can be grown using gas source molecular beam epitaxy (GSMBE) to achieve both *n*- and *p*-type materials with large optical gaps suitable for deep UV optoelectronic devices.^{6–8}

We describe here the use of SPSLs for preparing solar-blind *p-i-n* PDs and describe their characteristics. The PDs exhibit low dark leakage current density of ~3 pA/cm², high zero-bias resistance of ~6 × 10¹⁴ Ω, and peak responsivity of 62 mA/W at 247 nm under 10 V reverse bias.

The average composition and the resulting effective energy gap of AlN/AlGaN SPSL depends on the well/barrier thickness ratio, the well composition, and the SL period. Effective band gaps between 4.5 eV (276 nm) and 5.3 eV

(234 nm), as determined by optical reflectivity measurements,⁹ were obtained. Here, in order to compare the optical properties of our SPSLs with AlGaN random alloys, reflectance and transmittance were measured between 200 and 900 nm. Test SPSLs and AlGaN layers of comparable average AlN content (~70%) and total thickness (~400 nm) were grown using identical buffer layers (~40 nm thick AlN on sapphire) and without intentional doping. Using the method of Poruba *et al.*¹⁰ the reflectance and transmittance spectra were used to obtain the absorption coefficient (α) and index of refraction. Self-consistent expressions are numerically solved to obtain α at each photon energy ($\hbar\omega$). For transitions across direct band gap semiconductors, the absorption depends on photon energy according to

$$\alpha(\hbar\omega) \propto \sqrt{\hbar\omega - E_g} \quad (1)$$

just above the optical gap E_g . In Fig. 1 we graph α^2 versus photon energy, which is expected to rise linearly above E_g , for an AlGaN alloy layer. We note that the shapes of the alloy and superlattice absorption edges are comparable when the composition shift of E_g is taken into account. The magnitudes of the α^2 values are also consistent. For reference, Fig. 1 (inset) shows raw transmittance data for the same samples. These spectra are likewise comparable. A linear fit of α^2 versus photon energy data to $\alpha^2=0$ is used to estimate E_g . The conclusion from these studies is that SPSLs with extremely short period have optical absorption properties comparable to AlGaN random alloys, allowing us to apply similar design concepts for UV photodetectors.

Device structures were grown on 2 in. (0001) sapphire substrates using GSMBE with ammonia.¹¹ The growth started with an AlN nucleation layer, followed by an undoped ~300 nm thick SPSL with an average x_{AlN} content of

^{a)}Author to whom correspondence should be addressed; electronic mail: sergey.a.nikishin@ttu.edu

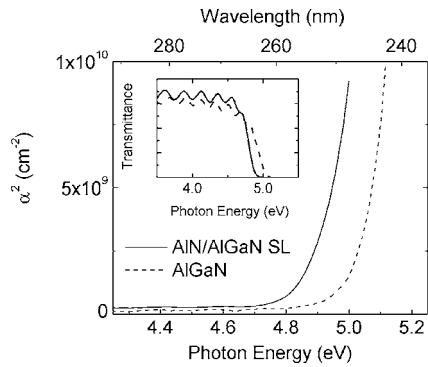


FIG. 1. Optical absorption spectra of AlN/Al_{0.08}Ga_{0.92}N SPSL and random AlGaIn alloy with similar average content of AlN and effective optical band gap. Inset shows the results of transmittance measurements for the same samples.

0.7 and transparent to 240 nm. These AlN and SPSL are required to mitigate dislocation density in the subsequent active layer of the device.^{8,12,13} The *n*-, *i*-, and *p*-type layers are composed of AlN/Al_{0.08}Ga_{0.92}N SPSLs having different optical gaps and thicknesses. These layers were grown in the two-dimensional (2D) growth mode. The SPSL growth rate was ~ 300 nm/h (0.33 ML/s) to ensure the fine control of the barrier and well thicknesses necessary to obtain optical band gaps from ~ 4.96 eV (~ 250 nm) in *i* layer to ~ 5.17 eV (~ 240 nm) in *n*- and *p*-type layers. The thicknesses of *n*, *i*, and *p* layers were varied in the range from 200 nm to 350 nm, from 40 to 120 nm, and from 100 to 250 nm, respectively. The SPSLs were either not intentionally doped (*i* type) or doped with Si derived from silane (*n* type), or Mg derived from effusion cell (*p* type).

A typical distribution of Si and Mg and SPSL optical band gaps through *p-i-n* part of photodetector structure are shown in Fig. 2. Using the dependences of E_g on SPSL period with 2 and 3 ML (monolayer) thick Al_{0.08}Ga_{0.92}N wells, reported in Refs. 8 and 9, one could estimate the period and well/barrier thicknesses of these SPSLs, namely ~ 9 ML (~ 2.25 nm) and ~ 3 ML (~ 0.75 nm)/ ~ 6 ML (~ 1.5 nm) and ~ 8 ML (~ 2 nm) and ~ 2 ML (~ 0.50 nm)/ ~ 6 ML (~ 1.5 nm) for *i* and *p* (*n*) regions, respectively. The average concentrations of Si and Mg measured by secondary ion mass spectrometry (SIMS) were $\sim 7 \times 10^{19}$ and $\sim 1 \times 10^{20}$ cm⁻³, respectively. Capacitance-voltage (*C-V*) measurements of the structure for which we show SIMS data in

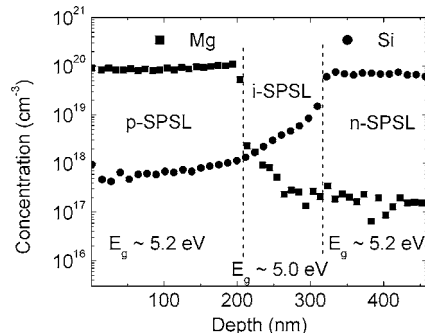


FIG. 2. SIMS profiles of Mg and Si for the *p-i-n* region of the double heterostructure 247 nm photodetector. Optical band gaps, E_g , of each region of device are shown.

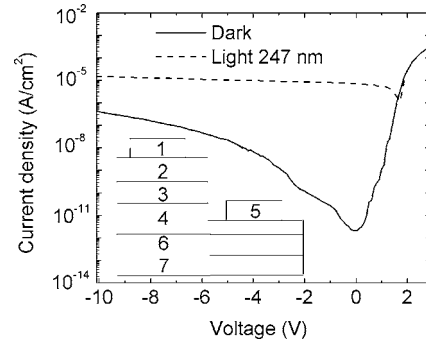


FIG. 3. Current-voltage characteristics of a photodiode in the dark (solid line) and under monochromatic 247 nm illumination (dashed line). Inset shows the schematic cross section of PD, where 1—Ni/Au contact, 2—*p*-SPSL, 3—*i*-SPSL, 4—*n*-SPSL, 5—Ti/Al/Ti/Au contact, 6—defect blocking SPSL, and 7—AlN buffer on sapphire substrate.

Fig. 2 reveal the width of the depletion region to be ~ 150 nm at zero bias. This result is consistent with ~ 110 nm *i*-region thickness shown by the vertical dashed lines in Fig. 2. The SIMS data illustrate substantial diffusion of the Si through the *i* region extending into the *p*-type layer. Although the impurity concentrations of Mg and Si in the *p*-type region differ by more than two orders of magnitude, activation of Si donors is more efficient than Mg acceptors. This could be one of the reasons for the high series resistance observed under forward bias for our *p-i-n* structure. The resulting nonuniform electric field across the *i* region could result in a diminished internal quantum efficiency of the PD.

In parallel experiments we studied the electrical properties of Si-doped ($N_D \sim 7 \times 10^{19}$ cm⁻³) and Mg-doped ($N_A \sim 1 \times 10^{20}$ cm⁻³) SPSLs with optical band gap of ~ 5.2 eV. Room temperature Hall measurements yielded an electron concentration $n \sim (3-5) \times 10^{19}$ cm⁻³ and mobility of ~ 30 cm²/V s for *n*-type layers and a hole concentration $p \sim (6-8) \times 10^{17}$ cm⁻³ and mobilities of 3–6 cm²/V s for *p*-type material. These results are consistent with a recent report on highly doped AlN/GaN SLs.¹⁴

Mesa photodiodes were prepared using standard processing. The 150 μ m diameter mesas were plasma etched with Cl₂ using 100 nm thick Ni hard masks.^{15,16} *p*- and *n*-type contacts were processed separately after removal of the Ni mask. *n*-type contacts were made using Ti/Al/Ti/Au with the total thickness of ~ 200 nm. Contacts to *p*-type SPSL were made using 50 nm of Ni followed by 70 nm of Au.

A representative current-voltage (*I-V*) characteristic of our PD structure is plotted in Fig. 3. Very low dark leakage current of ~ 0.5 fA is measured at near zero bias. This corresponds to the leakage current density of ~ 3 pA/cm² for the 150 μ m diameter mesa device. The reverse dark current remains below 0.5μ A/cm² up to a bias of -10 V and scales with the device area demonstrating the absence of significant contributions to leakage current from the device mesa sidewalls.² These extremely low values of dark current are comparable to the best results demonstrated for AlGaIn solar-blind PDs grown by MOCVD.¹⁻⁵ The dark current at lower bias, up to -1.5 V, does not significantly depend on applied voltage and exhibits a slope of $\sim 1-1.3$ in the log-log scale. We believe this low field leakage is due to tunneling of elec-

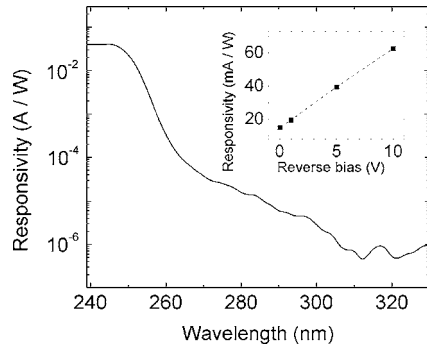


FIG. 4. Spectral responsivity of photodiode measured at -5 V reverse bias (bottom illumination). Inset shows responsivity vs reverse bias (247 nm illumination).

trons (holes) from the valence (conduction) band to the conduction (valence) band. The tunneling current is expected to depend on internal electric fields. Recent calculations¹⁷ have shown that the macroscopic polarization at heterojunction interfaces of AlN/AlGaIn SPSLs can be controlled, consistent with low leakage currents obtained in our devices.

At reverse bias over -3 V the dark current increases with exponent ranging, in different devices and wafers, from 3 to 6 in the log-log scale. Field-assisted thermal ionization of carriers from traps in the depletion region or combination of hopping conductivity and Poole-Frenkel effect are likely mechanisms for this conductivity.¹⁸ The range of slopes is typical of AlGaIn PDs at high reverse bias,^{1-6,13} and we believe the reverse current correlates with high defect density in structures grown on sapphire. The average density of threading dislocations in our samples, estimated from x-ray measurements, is $\sim 10^9$ cm⁻². This is comparable to that reported for AlGaIn grown by MOCVD over thin AlN buffer on sapphire.¹⁻³

From (dV/dI) we calculate zero-bias PD resistance of $\sim 6 \times 10^{14}$ Ω , resulting in the area-resistance product $R_0A \sim 1.2 \times 10^{11}$ Ω cm². The PD exhibits excellent monochromatic photoresponse at 247 nm, with $I_{247 \text{ nm}}/I_{\text{dark}} \sim 3 \times 10^6$ at zero bias, as shown in Fig. 3.

The spectral responsivity of PDs under reverse bias is shown in Fig. 4. The peak response was obtained at a wavelength of ~ 247 nm, in excellent agreement with the expected optical band gap of ~ 5 eV for the *i* region of the PD. The device shows excellent rejection of visible radiation. Cutoff at 247 nm is obtained for these devices, with three orders of magnitude decrease in responsivity from 247 to 265 nm and four orders of magnitude rejection by 315 nm. This compares well with the rejection ratios in state-of-the-art *p-i-n* PDs with cutoff at longer wavelength.¹⁻⁵ The substructure visible in the photoresponse in the range of ~ 265 – 315 nm is not understood at this time. It may be related to broadening of the absorption edge due to partial monolayer thickness fluctuations in the well and barrier thickness and formation of the well/barrier interfacial layers with intermediate AlN content. Furthermore, there is little information regarding the effect of intentional doping on the optical absorption properties of AlGaIn, which may result in

an Urbach tail and affect the device efficiency and spectral response. A study of the temperature dependence of the PD spectral response is needed to examine this hypothesis.

At zero bias the responsivity of 16 mA/W was measured at a wavelength of 247 nm. This corresponds to an external quantum efficiency of $\sim 12.5\%$. The responsivity linearly increases with reverse bias, as shown in the inset of Fig. 4, and reaches its maximum value of 62 mA/W at -10 V. This corresponds to an external quantum efficiency of 30%. This is less than the highest responsivity reported in solar-blind *p-i-n* PD of $\sim 72\%$ at 282 nm Ref. 13 grown by MOCVD. Optimizing the dopant distribution throughout the device, but particularly in the *i* region, should improve the external quantum efficiency of our PDs. Nevertheless, using the R_0A determined above we calculate the thermal noise limited specific detectivity, at zero bias, of $D^* = 4.5 \times 10^{13}$ cm Hz^{1/2} W⁻¹.

In summary, we have prepared solar-blind heterostructure *p-i-n* photodetectors based on short period superlattices. Excellent electrical characteristics of *p-n* junctions formed in these SPSLs demonstrate their potential in solar-blind avalanche photodetectors.

The authors would like to thank Professor H. Temkin for important discussions. Work at Texas Tech University is supported by NSF (ECS-0323640 and ECS-0304224) and the J. F. Maddox Foundation.

¹R. D. Dupuis and J. C. Campbell, in *Wide Energy Bandgap Electronic Devices*, edited by F. Ren and J. Zolper (World Scientific, Singapore, 2003), and references therein.

²H. Temkin, in *Advanced Semiconductor and Organic Nano-techniques Part I*, edited by H. Morkoç (Academic, San Diego, 2003), and references therein.

³E. Monroy, F. Omnès, and F. Calle, *Semicond. Sci. Technol.* **18**, R33 (2003), and references therein.

⁴E. Ozbay, N. Biyikli, I. Kimukin, T. Kartaloglu, T. Tut, and O. Aytür, *IEEE J. Sel. Top. Quantum Electron.* **10**, 742 (2004), and references therein.

⁵M. B. Reine *et al.*, *Proc. SPIE* **6121**, 237 (2006).

⁶V. Kuryatkov, A. Chandolu, B. Borisov, G. Kipshidze, K. Zhu, S. Nikishin, H. Temkin, and M. Holtz, *Appl. Phys. Lett.* **82**, 1323 (2003).

⁷S. A. Nikishin, V. V. Kuryatkov, A. Chandolu, B. A. Borisov, G. D. Kipshidze, I. Ahmad, M. Holtz, and H. Temkin, *Jpn. J. Appl. Phys., Part 2* **42**, L1362 (2003).

⁸S. A. Nikishin, M. Holtz, and H. Temkin, *Jpn. J. Appl. Phys., Part 1* **44**, 7221 (2005).

⁹M. Holtz, I. Ahmad, V. V. Kuryatkov, B. A. Borisov, G. D. Kipshidze, A. Chandolu, S. A. Nikishin, and H. Temkin, *Mater. Res. Soc. Symp. Proc.* **798**, Y1.9.1 (2004).

¹⁰A. Poruba *et al.*, *J. Appl. Phys.* **88**, 148 (2000).

¹¹G. Kipshidze, V. Kuryatkov, B. Borisov, S. Nikishin, M. Holtz, S. N. G. Chu, and H. Temkin, *Phys. Status Solidi A* **192**, 286 (2002).

¹²H. Wang, J. Zhang, C. Chen, Q. Fareed, J. Yang, and A. Khan, *Appl. Phys. Lett.* **81**, 604 (2002).

¹³R. McClintock, A. Yasan, K. Mayes, D. Shiell, S. R. Darvish, P. Kung, and M. Razeghi, *Appl. Phys. Lett.* **84**, 1248 (2004).

¹⁴S. Yamaguchi *et al.*, *Appl. Phys. Lett.* **80**, 802 (2002).

¹⁵V. V. Kuryatkov, G. D. Kipshidze, S. A. Nikishin, P. W. Deelman, and H. Temkin, *Phys. Status Solidi A* **188**, 317 (2001).

¹⁶K. Zhu, V. Kuryatkov, B. Borisov, G. Kipshidze, S. A. Nikishin, H. Temkin, and M. Holtz, *Appl. Phys. Lett.* **81**, 4688 (2002).

¹⁷K. A. Bulashevich and S. Yu. Karpov, *Phys. Status Solidi C* **2**, 2394 (2005).

¹⁸D. V. Kuksenkov, H. Temkin, A. Osinsky, R. Gaska, and M. A. Khan, *J. Appl. Phys.* **83**, 2142 (1998).